Alzheimer's & Dementia: Translational Research & Clinical Interventions 1 (2015) 170-181

Featured Article

Pharmocologic treatment with histone deacetylase 6 inhibitor (ACY-738) recovers Alzheimer's disease phenotype in amyloid precursor protein/presenilin 1 (APP/PS1) mice

Tabassum Majid[a], Deric Griffin[a], Zachary Criss, II[a], Matthew Jarpe[b], Robia G. Pautler[a,c,d,*]

[a]*Interdepartmental Program in Translational Biology and Molecular Medicine, Baylor College of Medicine, Houston, TX, USA*
[b]*Acetylon Pharmaceuticals, Boston, MA, USA*
[c]*Department of Molecular Physiology and Biophysics, Baylor College of Medicine, Houston, TX, USA*
[d]*Department of Neuroscience, Baylor College of Medicine, Houston, TX, USA*

Abstract

Introduction: Current therapy for Alzheimer's disease (AD) focuses on delaying progression, illustrating the need for more effective therapeutic targets. Histone deacetylase 6 (HDAC6) modulates tubulin acetylation and has been implicated as an attractive target. HDAC6 is also elevated in postmortem tissue samples from patients. However, HDAC6 inhibitors have had limited success preclinically due to low blood-brain barrier penetration.

Method: We investigated a specific, potent HDAC6 inhibitor (ACY-738) in a mouse model of AD. We determined the effects of ACY-738 treatment on axonal transport, behavior, and pathology in amyloid precursor protein/presenilin 1 mice.

Results: We demonstrated improvements in in vivo axonal transport in two treatment groups as a result of ACY-738 brain levels. We also demonstrated recovery of short-term learning and memory deficits, hyperactivity, and modifications of tau and tubulin.

Discussion: Our findings implicate specific, targeted HDAC6 inhibitors as potential therapeutics and demonstrate that further investigations are warranted into effects of HDAC6 inhibitors in AD.

Keywords: HDAC6; Alzheimer's disease; Axonal transport; Acetylated tubulin; Microtubule; Therapeutic; Preclinical; ACY-738

1. Introduction

Alzheimer's disease (AD) is a progressive, neurodegenerative disorder that affected over 5 million people in the United States alone last year [1]. The prevalence of this disease is projected to double by the year 2040. Currently, patients can be diagnosed with probable AD with a combined profile of positron emission topography imaging, cognitive score, and genetic analysis. However, a confirmation of the three pathologic hallmarks of the disease (amyloid-beta [Aβ] plaques, neurofibrillary tau tangles, and neurodegeneration) cannot be fully assessed unless an autopsy is performed. Current Food and Drug Administration-approved therapeutics for management of the symptoms of this disease primarily include cholinesterase inhibitors [2]. In addition, drugs that target two pathologic hallmarks (Aβ plaques and neurofibrillary tau tangles) of the disease have been explored. Specifically, small molecule inhibitors of Aβ aggregation or production are under development and have had mixed results in clinical trials [3]. Inhibitors of tau-induced neurotoxicity such as inhibitors of kinases (CDK5, GSK3β) have also been explored with limited success, often due to their lack of brain bioavailability. These include targeting either the

*Corresponding author. Tel.: +1-713-798-5705; Fax: +1-713-798-3475.
E-mail address: rpautler@bcm.edu

http://dx.doi.org/10.1016/j.trci.2015.08.001

phosphorylation or the aggregation of tau before aggregation and the formation of filamental tangles [4]. Even more recently, increased attention has been paid to the biological role of tau in microtubule stabilization, which is a vital structure for the health of axons in the brain. Several studies have investigated the crucial role of axons and their ability to transport organelles and vesicles to and from synapses in neurons via microtubules [5–7]. In fact, recent studies [8,9] describe the damage of several components of microtubules in neurodegenerative disease, specifically with genetic mutations in common cytoskeletal and motor components of microtubules [9].

Microtubules are composed mainly of two polymer proteins, α- and β-tubulin [10]. These proteins are regulated by posttranslational modifications (PTMs) including acetylation and phosphorylation. These PTMs can play crucial roles in the stability, guidance, and transport that take place along these axons. Because of this, the physiological process of microtubule-based axonal transport is of great interest as a functional indicator of neuronal health.

We and others have shown that microtubule-based axonal transport can be measured directly in vivo in models of AD using manganese-enhanced magnetic resonance imaging (MEMRI) [11–15]. Over the past 20 years, this technique has been used in vivo in rodent models to confirm in vitro and ex vivo impairments in axonal transport rate [12–14,16–18]. Thus, the MEMRI technique offers an in vivo methodology for microtubule-based axonal transport. Furthermore, microtubule-destabilizing agents (i.e., colchicine) can be used in vivo to confirm blockage of axonal transport using MEMRI. Recent studies have confirmed in vivo deficits in microtubule-based axonal transport are present before the onset of tau tangles in tauopathy models [13,16]. These deficits are highly correlated with PTMs of tau.

In addition to tau, tubulin is another key building block within microtubules that can be acetylated or deacetylated by histone deacetylase 6 (HDAC6) [19]. Evidence in patient samples indicates that this regulation is disrupted because of the level of HDAC6 being elevated in the brains of patients with AD, specifically by 52% in the cortex and 91% in the hippocampus, which is the center for learning and memory [20,21]. In addition, levels of acetylated α-tubulin protein are decreased in AD patient brains. HDAC6 has also been shown to interact with tau independent of its deacetylase activity and also helps to recruit chaperone proteins within the autophagic process to help clear protein aggregates. Studies also indicate that HDAC6 can directly modulate the phosphorylation and acetylation of tau as a protein [19,21,22]. These functions have been demonstrated in recent studies in multiple models of AD [21,23–26].

Because of the various functions of HDAC6 in neurons and its potential as a therapeutic target, a number of inhibitors have been developed. The first of these includes tubacin, which is specific to the α-tubulin regulation and to HDAC6; however, it has high lipophilicity and is difficult to synthesize [10,27]. The second is tubastatin A and its respective group of analogs. This family of drugs is less lipophilic and more selective for HDAC6 and its deacetylase activity, but dosing mice with this compound did not result in significant brain exposure [28]. However, a recent study compared these two inhibitors and did find that tubastatin A was most effective in the peripheral nervous system at rescuing distal axonal loss and muscle innervation in mouse models of Charcot-Marie-Tooth disease [29]. Most recently, Acetylon Pharmaceuticals has developed a series of selective and potent HDAC6 inhibitors that efficiently cross the blood-brain barrier. In a recent study, one of the compounds in this series, ACY-738, resulted in an antidepressant-like phenotype in a social defeat model of depression in mice. Thus, we sought to evaluate the effectiveness of ACY-738 in an amyloid mouse model of AD on axonal transport, behavior, and amyloid pathology.

Specifically, we chose the amyloid precursor protein/presenilin 1 (APP/PS1) mouse model because of the relevance of increased amyloid as an early marker of cognitive impairment in patients and in mice. In addition, amyloid has been highly associated with impairments in axonal transport and microtubule instability. Reduced axonal transport has been correlated with poor behavioral outcomes in mouse models of AD [8,12,30]. These correlations have linked Aß with tau proteins within dystrophic axons, leading to deficits in axonal transport. In addition, axonal transport deficits have been implicated as triggers for increased oxidative stress, and can lead to higher Aß deposition over time. Many of the proteins involved with this processing, including APP and PS1 have been observed to be accumulated in axons at presynaptic terminals, indicating that this transport process is necessary in the delivery of these cargo [31,32]. Specifically, the process of fast anterograde axonal transport is responsible for the delivery of these proteins. In addition, evidence suggests that APP directly interacts with kinesin in the development of microtubules and promotes axonal growth. Additional in vitro evidence of APP and PS1 manipulation in cell culture leads to altered axonal growth, morphologic changes, and swelling within neurons [33,34]. Finally, the APP/PS1 mouse model has been characterized using the MEMRI methodology for measurements of noninvasive, in vivo axonal transport rates, with rates decreasing beginning at age 3 months before overt biochemical changes in pathology as well as learning and memory deficits. Thus, we chose to evaluate the effects of ACY-738 at this time point, referred as 21 day or early treatment throughout the article. We selected a longer, 90-day treatment beginning at 3 months and evaluated at 6 months, referred to as the late or 90-day treatment throughout the article. Finally, axonal transport deficits have been linked to oxidative stress abnormalities before the onset of plaque depositions, all of which affect the microtubule network which ACY-738 targets through HDAC6 inhibition.

2. Methods

2.1. Animal model and genotyping

APP/PS1 mice that overexpress both the APP and PS1 with a deletion in exon 9 have been described previously [35]. The transgenic mice were gifts from Hui Zheng (Baylor College of Medicine), and male breeders were crossed with wild-type (WT) C57/Bl6J females from Jackson Laboratories. For all groups, both male and female mice were used, and pilot studies were conducted before data collection to confirm no sex differences in these measurements. Mouse genotypes were determined from tail tissue from mice using real-time quantitative polymerase chain reaction with specific probes for the *PSEN1* gene by a commercial provider. To perform the genotyping, tissues from mice were digested in extraction buffer (components of buffer) at 75°C for 5 minutes and vortexed. They were then digested for 10 minutes at 95°C before DNA was extracted. Polymerase chain reaction cycling conditions were as follows: 95°C for 3 minutes, 95°C for 15 seconds, 62°C for 15 seconds, 72°C for 20 seconds, and 95°C for 3 minutes for 34 cycles. Animal housing and use were in compliance with the National Institutes of Health guidelines for the Care and Use of Laboratory Animals and were approved by the Institutional Animal Care and Use Committee at Baylor College of Medicine.

2.2. Contextual fear conditioning

Contextual fear conditioning tests were conducted in the same manner as previously described [36]. Briefly, mice were first habituated for 30 minutes in the behavioral suite and then placed in fear conditioning chambers. A training protocol was administered using Freeze Frame software (Coulbourn Instruments), which consists of two instances of a low tone paired with a mild electric foot shock (0.7 mA) in a 3-minute time frame. The amount of time that the mice were immobile, designated as "freezing" in this protocol was recorded by the software. For short-term recall, mice were placed back in the same chamber without a tone or foot shock, to measure contextual fear conditioning 2 hours after testing. For long-term recall, mice were again placed in the same chamber 24 hours after testing. Both outputs were measured using Freeze View software (Coulbourn Instruments) after individually adjusting a baseline freezing threshold for each mouse that was tested.

2.3. Manganese administration

Mice were anesthetized with 5% isoflurane in 100% O_2 for 2 minutes to administer a nasal lavage of 4 μL of 0.75-g/mL $MnCl_2$ dissolved in nanopure water. Once this was administered, the animals were placed back into their cage and allowed to recover. One hour after lavage administration, the mice were exposed to 5% isoflurane and then carefully exposed to 2% isoflurane in 100% O_2 for imaging. Mice were then placed in a head holder while respiratory rate was monitored and temperature was maintained at 37°C. This was done using an air heating system with the Model 1025 Small Animal Monitoring and Gating System Software (SA Instruments, Inc).

2.4. Magnetic resonance imaging

All images in this study were acquired with a 9.4-T Bruker Avance BioSpec spectrometer, 21-cm bore horizontal scanner with a 35-mm volume resonator (Bruker BioSpin, Billerica, MA, USA). Imaging parameters of the olfactory MEMRI scans were as follows: echo time = 8.536 ms, relaxation time = 504 ms, field of view = 30 mm^2, slice thickness = 1 mm, matrix = 128 × 128, number of excitations = 2, and number of cycles = 15 (each cycle taking about 2 minutes) to acquire using ParaVision software (Bruker BioSpin). The scan was a RARE sequence scan that was modified to have six slices per cycle. The first slice was consistently aligned at the most posterior point of the olfactory bulb to ensure slice reproducibility from mouse to mouse for the MEMRI scans.

2.5. Magnetic resonance imaging data analysis

All scans were analyzed using ParaVision software (Bruker BioSpin). The length of the olfactory bulb was measured and a line was placed on the image. From the midpoint of this line, a 90° angle was drawn, extending outward toward the olfactory neuronal layer (ONL), where the region of interest (ROI) was selected. Signal intensity was measured in a ROI of one pixel in the ONL on the right side of the olfactory bulb because of a chemical shift artifact present on the left side of the bulb [12,37]. One pixel was selected because of the pixel representing one fascicle of axons that project into the ONL. Single glomeruli are the target of these fascicles and one pixel minimizes outside variation from other fascicles within the olfactory epithelium [38]. Another ROI of nine pixels was used to measure signal intensity in the water phantom. All ONL ROIs were normalized to water phantom ROIs for 15 measurements, which correspond to the 15 cycles in the scan to account for any differences in intensities from experiment to experiment. This normalized signal intensity was used to plot 15 measurements per mouse. The slope of this line was then established as the axonal transport rate for each mouse. For statistical analysis, two-tailed Student *t* tests was used to test for differences between WT and APP/PS1 mice with each set of axonal transport measurements (early and late cohorts).

2.6. Serum processing

Mice were briefly anesthetized before performing a retro-orbital bleed. Blood was collected from 6-month-old mice (late cohort) using heparinized coated tubes (Fisher). Plasma was isolated by centrifuging blood samples at 7800 rpm for

7 minutes at 4°C. Plasma samples were snap-frozen on dry ice and stored at −80°C until use.

2.6.1. Brain tissue processing

Mice were sacrificed at ages 3 and 6 months for the early and late cohorts, respectively. The brain was dissected and divided into cortex, hippocampus, olfactory bulb, and cerebellum. These parts were then kept at −80°C until use. For enzyme-linked immunosorbent assay (ELISA) assays, hippocampal tissues were homogenized in lysis buffer consisting of radioimmunoprecipitation assay and 1-mM ethylenediaminetetraacetic acid (EDTA) and prepared according to the protocol from BetaMark ELISA Kit SIG-38952 or 38954 (Covance). For protein extraction, tissues were homogenized in lysis buffer consisting of 50-mM Tris (pH 7.5), 150-mM NaCl, 1-mM EDTA (pH 8.0), 1-mM phenylmethylsulfonyl fluoride, 1% Triton X-100, protease inhibitor cocktail (Sigma, St Louis, MO, USA), and phosphatase inhibitor cocktail (Roche Applied Science, Indianapolis, IN, USA). Total protein concentration was measured using the Bradford Reagent (Thermo Scientific/Pierce Biotechnology, Rockford, IL, USA).

Ten micrograms of total protein lysate per sample were resolved by sodium dodecyl sulfate polyacrylamide gel electrophoresis and transferred onto a nitrocellulose membrane, and probed with antibodies against glyceraldehyde 3-phosphate dehydrogenase (1:2000, Abcam), mHDAC6 (1:2000, Abcam), human tau (1:2000, Abcam), acetylated tubulin (1:1000, Cell Signaling), and pSer262 Tau (1:2000, Millipore). Western blot analysis was performed with infrared dye–conjugated secondary antibodies, IR700 and IR800 (LI-COR Biosciences, Lincoln, NE, USA). Blots were imaged and processed on an Odyssey Infrared Imaging System.

2.7. Drug administration and pharmacokinetic measurements

Like many hydroxamic acid–based compounds, ACY-738 demonstrates a relatively short half-life when injected intraperitoneally (IP) in mice [8]. To avoid the repeated stress of twice daily IP injections, we developed a rodent chow–based formulation of the compound. The level of ACY-738 in chow was based on extensive pharmacokinetic studies performed in rats. When dosed orally at 10 mg/kg, ACY-738 achieves a maximum plasma concentration of 212 ng/mL (79 nM) with a half-life of 2.2 hours. In cell-based assays (data not shown), a concentration of between 10 and 100 nM induces a significant acetylation of α-tubulin with little acetylation of histones, indicating that this concentration range is selective for HDAC6 over class I HDACs (data not shown). Therefore, we calculated that the amount of drug in the chow should be sufficient to deliver 10 mg/kg × 24/2.2 hours or 100 mg/kg. Calculating that mice consume 4 g of chow per day, we formulated Harlan Teklad diet 7012 to contain 0.625 mg of ACY-738 per gram of chow (4 g × 0.625 mg = 2.5 mg/0.025 kg per mouse = 100 mg/kg). Mice were weighed weekly to monitor overt toxicity of diet-based treatment of ACY-738. For PK analyses, ACY-738 was measured in plasma and brain by liquid chromatography/tandem mass spectrometry. Drugs were extracted from brain and plasma by protein precipitation using 50: 50 acetonitrile:methanol and analyzed using a high performance liquid chromatography/mass spectrometry (HPLC/MS/MS) method using electrospray ionization in positive mode as previously reported [28]. The lower limit of quantification for all compounds was 3 ng/mL. PK parameters (concentrations, $T_{1/2}$, concentration (AUC) AUC_{Brain}/AUC_{Plasma}) were estimated by noncompartmental model using WinNonlin (Pharsight, Sunnyvale, CA, USA).

2.8. Enzyme-linked immunosorbent assays

Hippocampal tissue was isolated from 3- and 6-month-old mice (early and late treatment groups, respectively) and kept until −80°C until use. Tissue was homogenized in 1× tris buffered saline with protease and phosphatase inhibitors and EDTA. Homogenates were then spun at 4°C at a speed of 350,000 × *g* using tabletop ultracentrifuge (Beckman Coulter). Supernatants were isolated and used at 1:2 dilutions for the assay. Plasma samples were isolated from both groups using retro-orbital bleeds, as described previously, and were also diluted at 1:2 for the assay. Colorimetric ELISA kits specific for Aβ 1–40 (Covance) and 1–42 (Covance) were used to measure total amyloid in both brain and plasma samples.

2.9. Immunohistochemistry

APP/PS1 and WT littermate mice (6-month-old) were anesthetized with 5% isoflurane and euthanized using cervical dislocation. The brain was dissected and half was immediately placed in 10% formalin for postfixation, whereas the other half was snap-frozen and used for biochemical analysis as described in Section 2.6. The samples were rinsed with 1× phosphate-buffered saline, transferred to one wash of 50% ethanol for 1 hour, then 70% ethanol overnight. The samples were then embedded in paraffin. The samples were then sectioned along the sagittal plane at 20-μm thickness and directly mounted onto precleaned/coated slides. The sections were stained with Aβ antibody 1–42 (Invitrogen) after formic acid treatment. The sections were also stained with Congo red to visualize plaque cores. Slides were imaged using META 510 Confocal Microscope (Zeiss).

3. Results

3.1. ACY-738 treatment improves axonal transport rates in early and late treatment groups

Both APP/PS1 mice and WT littermates were assigned randomly to either treated or untreated groups for the course of this study. In both early and late treatment groups, mice

were fed for 21 days with normal mouse chow (untreated) or ACY-738 chow (treated) and weighed weekly to monitor overt toxicity. Weight from treated and untreated APP/PS1 and WT mice are displayed in Supplementary Fig. 1A and B. There are no significant differences in weight gain between treated and untreated groups.

In both groups, axonal transport measurements were conducted using MEMRI as described previously [13]. In 3-month-old mice, axonal transport deficits for APP/PS1 mice are 65% of WT mice. Treatment of WT mice had no effect on axonal transport rates (Fig. 1A). After 21 days of ACY-738 treatment, APP mice exhibited axonal transport rates that were comparable to WT animals. In 6-month-old mice, axonal transport deficits for APP-untreated mice are 38% of WT untreated mice (Fig. 1B). Treatment with ACY-738 for 3 months significantly recovered axonal transport deficits for APP/PS1 mice.

3.2. ACY-738 is present at therapeutic levels in the brain and plasma of APP/PS1 mice

ACY-738 levels were measured in plasma and cortical samples from all treatment groups using HPLC (n = 3 per group). In the early group, untreated mice displayed ACY-738 levels that were below quantifiable limits for both plasma and brain samples. In cortical samples, treated mice displayed an average of 16.07 (WT) and 17.93 nanograms of ACY-738 per gram of tissue (59 and 66 nM; Fig. 2A). When examining the plasma drug levels, WT- and APP-treated groups contained an average of 22 and 27.07 ng/mL of ACY-738, respectively (81 and 100 nM; Fig. 2A). In the late-treatment group, all untreated mice displayed ACY-738 levels that were below quantifiable limits for both plasma and brain samples. In cortical samples, treated WT mice displayed an average of 17.80 ng/g (WT) and 14.20 ng/g (APP) of ACY-738 per gram of tissue (66 and 52 nM; Fig. 2B). In the plasma, both WT- and APP-treated groups contained an average of 40.35 and 50 ng/mL of ACY-738, respectively (149 and 185 nM; Fig. 2B). The higher levels of drug in the older animals likely represent a different rate of metabolism of the drug. ACY-738 is rapidly converted from a hydroxamic acid to a carboxylic acid, most likely through a glucuronide intermediate, by enzymes in the liver. The carboxylic acid has no HDAC inhibitory activity (data not shown).

3.3. ACY-738 treatment elevates protein levels of acetylated tubulin while lowering levels of hyperphosphorylated tau protein

Cortical samples from treated and untreated APP/PS1 mice and WT littermates were isolated, and a Western blot was used to measure protein levels of acetylated α-tubulin, α-tubulin, GAPDH, human tau, and phosphorylated tau Ser262. Untreated APP/PS1 mice displayed significantly lower levels of acetylated tubulin when compared with

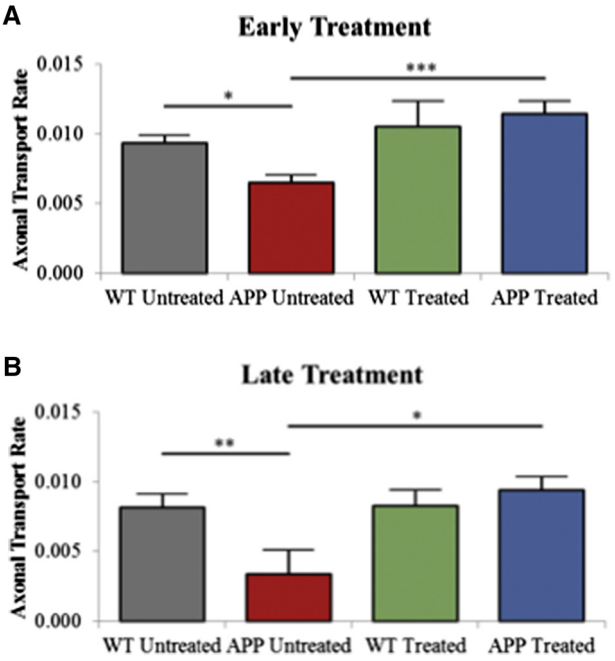

Fig. 1. Axonal transport rates are improved in both early and late treatment groups. Quantification of axonal transport rate is displayed for mice treated for (A) 21 d before evaluation at the age of 3 mo for all groups and (B) for mice treated for 90 days before evaluation at the age of 6 months. WT untreated n = 8 (early), 10 (late), APP untreated n = 6 (early), 11 (late), WT treated n = 4 (early), n = 5 (late), APP treated, n = 8 (early), n = 9 (late). Two-way ANOVA was conducted with multiple comparisons, $*P < .05$, $**P < .01$, $***P < .005$. Abbreviations: WT, wild-type; APP, amyloid precursor protein; ANOVA, analysis of variance.

WT mice, and these levels were significantly elevated after an early treatment with ACY-738. A visual representation of these Western blots and their quantification are displayed in Fig. 3A. We also measured hyperphosphorylated tau levels at Ser262 and normalized these levels to tau and GAPDH as a loading control. Untreated APP/PS1 mice display slightly elevated levels of hyperphosphorylated tau at Ser262, which are normalized to WT levels after an early treatment with ACY-738 chow. A representative Western blot and their quantification are displayed in Fig. 3B. This is similar to the reduction in phosphorylated tau seen with a 0.5-mg/kg injection of ACY-738 [38].

3.4. ACY-738 treatment improves hyperactivity and fear-associated contextual learning and memory

Only mice from the late-treatment groups were evaluated using both an open field assay and short-term and long-term contextual fear conditioning paradigms because of no reported behavioral deficits ssin APP/PS1 mice at age 3 months. APP/PS1-untreated mice traveled much further (197.2 m) compared with WT-untreated mice (94.21 m). There was no change in WT mice treated with ACY-738 chow (101.6 m); although APP/PS1-treated mice showed recovery back to WT levels (122 m) groups (Fig. 4A). In the contextual fear conditioning assay,

A

Early Treatment (21 days)	Brain (ng/g)	Plasma (ng/mL)	ACY-738 Brain/ Plasma
WT Untreated	1	1	1
APP Untreated	1	1	1
WT Treated	22 ± 4.07*	16.07 ± 2.18**	1.39
APP Treated	27.07 ± 2.98*	17.93 ± 3.00**	1.51

B

Late Treatment (90 days)	Brain (ng/g)	Plasma (ng/mL)	ACY-738 Brain/ Plasma
WT Untreated	1	1	1
APP Untreated	1	1	1
WT Treated	40.35 ± 12.05***	17.80 ± 4.20	0.44
APP Treated	50.00 ± 11.85***	14.20 ± 1.68	0.28

Fig. 2. ACY-738 is present in the brain and plasma of treated mice in both early and late groups. Quantification of samples from plasma and brain tissue is displayed (A) for the early treatment group and (B) for the late treatment group. n = 3 for all groups, one-way ANOVA was performed for both early and late treatment groups; significance is indicated for treated to untreated groups, $*P < .05$, $**P < .01$, $***P < .005$. Abbreviations: ANOVA, analysis of variance; WT, wild-type; APP, amyloid precursor protein.

APP/PS1-untreated mice have a significantly lower percent freezing compared with the WT-untreated group, with an average of 21% and 30%, respectively (Fig. 4B). The results of a short-term (2 hours posttraining) recall paradigm illustrate a significant recovery in contextual fear–associated memory deficits, with the percent freezing

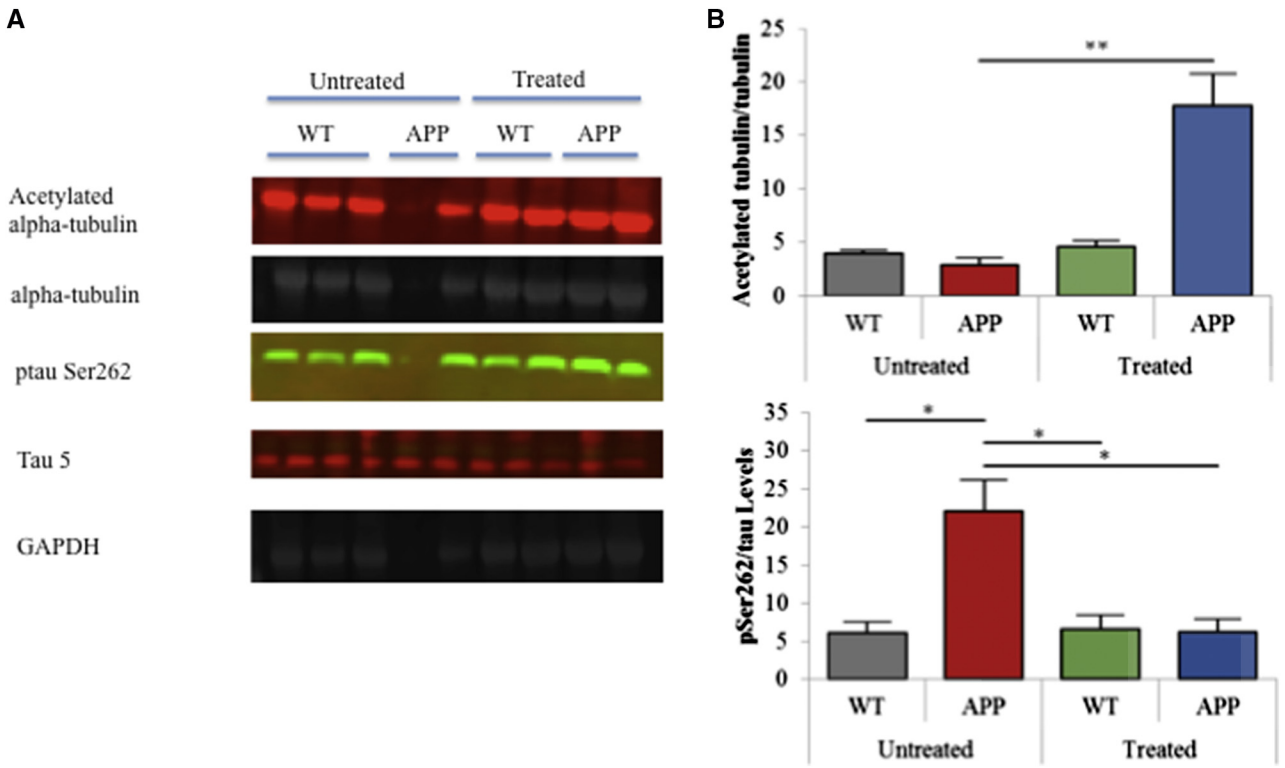

Fig. 3. A) Cortical brain tissue was collected from all treatment groups and processed for Western blots, n = 3 per group. Samples displayed were probed with an anti-taupSer262 antibody (1:1000) tau 5 antibody (1:2000), acetylated tubulin antibody (1:2000), α-tubulin antibody (1:5000), and GAPDH (1:2000) and imaged using the LI-COR System (Odyssey) and B) quantified using ImageJ (NIH). One-way ANOVA test was conducted, $*P < .05$, $**P < .01$. Abbreviations: ANOVA, analysis of variance; WT, wild-type; APP, amyloid precursor protein.

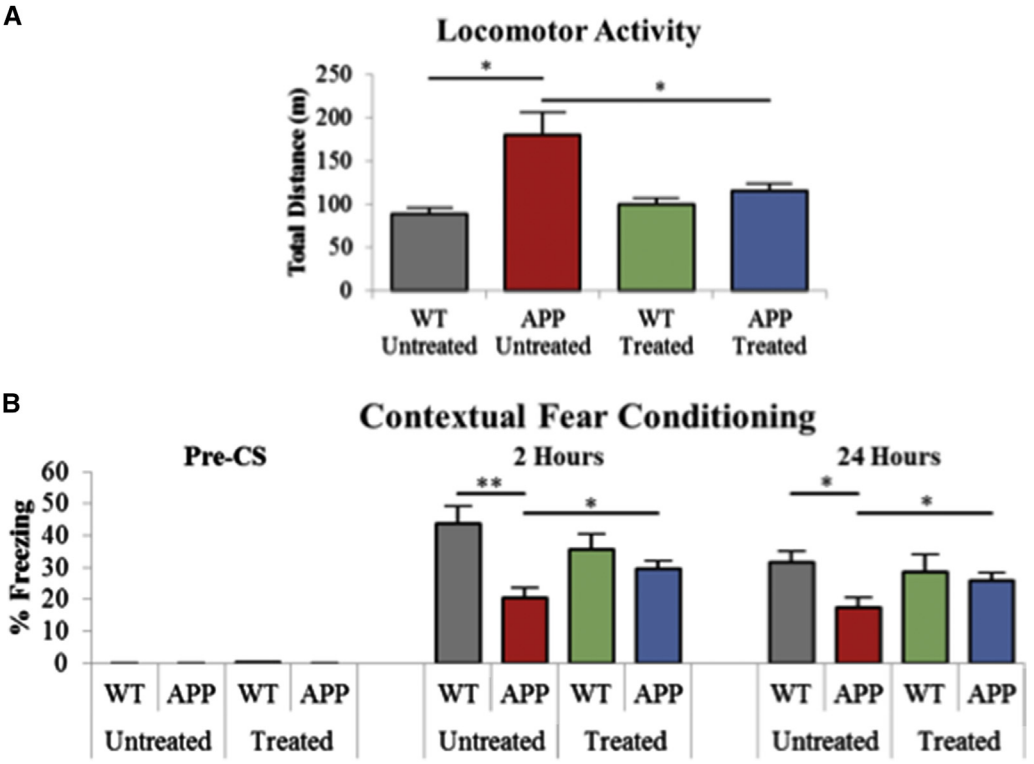

Fig. 4. WT and APP/PS1 mice (male and female, 6–7 mo old) were treated with normal or ACY-738 chow for 90 d before testing using an open field assay for 30 min and contextual fear conditioning paradigm. Results are reported for total distance traveled in the open field (A) and as % freeze as an indication of fear-associated memory recall. Graph displays preconditioned stimulus (pre-CS), short-term recall (2 h), and long-term recall (24 h) (B). Groups tested include WT untreated (n = 20), APP/PS1 untreated (n = 13), WT treated (n = 13), and APP treated (n = 15). Two-way ANOVA was conducted with multiple comparisons. $^{*}P < .05$, $^{**}P < .01$. Abbreviations: WT, wild-type; APP/PS1, amyloid precursor protein/presenilin 1; ANOVA, analysis of variance.

for the WT-treated group measured as 30% and as 22% for the APP/PS1-treated group (Fig. 4B). When mice were placed in a long-term (24 hours posttraining) recall paradigm, the deficit in learning and memory was even more significant between the untreated groups, with percent freezing of WT mice at 30% and APP mice at 15%. There is a significant recovery of long-term recall, with 20% for the WT-treated group and 25% for the APP-treated group (Fig. 4B).

3.5. ACY-738 treatment improves amyloid pathology in APP-treated mice

We used an ELISA to quantify the levels of human Aβ 1–40 and 1–42 in all late-treatment groups in the cortex of both treated and untreated mice. Both soluble and insoluble Aβ 1–42 levels were significantly elevated in APP-untreated mice compared with WT, and ACY-738 treatment significantly decreased the levels of insoluble Aβ 1–42 (Fig. 5A). This was also confirmed when calculating the Aβ 42/40 ratios, which indicated that the insoluble ratio was significantly decreased in the treated APP mice (Fig. 5B). To confirm the pathology visually, we stained brain slices from the late-treatment cohort with an amyloid 1–42 antibody, which revealed an average of seven plaques per slice in APP-treated mice compared to one plaque per slice in APP-untreated mice. Representative images of APP untreated, treated, and plaque histology are displayed in Fig. 6A. Plaque staining quantification is indicated in Fig. 6B. Soluble amyloid puncta (neuritic plaque cores) were also imaged using Congo red. Representative images are displayed in Fig. 6C. Puncta quantification is indicated in Fig. 6D.

4. Discussion

A reduction of fast axonal transport associated with neurodegenerative disease has been well established. The involvement of HDAC6 in this process has been demonstrated in vitro [23,39]. Here, we demonstrate the role of HDAC6 in fast axonal transport in vivo and link this effect to behavioral consequences.

We evaluated the effectiveness of a novel, specific HDAC6 inhibitor (ACY-738) in a preclinical proof-of-concept study using APP/PS1 mice. From a close examination of previous literature, we constructed a model indicating the role of HDAC6 and its interactions in healthy and diseased neurons (Fig. 7). Specifically in the context of drug development, class I HDAC inhibitors have been used in humans primarily for cancer. This is due to the observation that when compared with class I inhibitors, class II HDACs are downregulated in tumor samples. In addition, the higher the expression of this class of HDACs, the

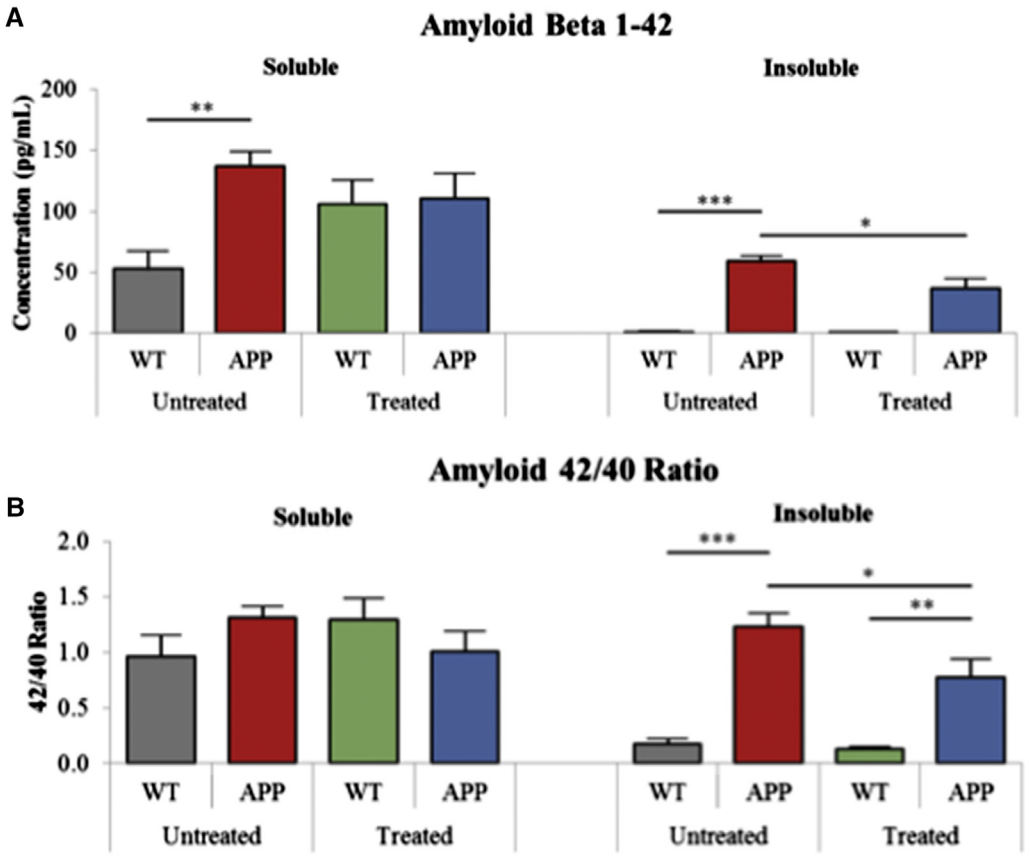

Fig. 5. Insoluble 1–42 levels are significantly reduced after ACY-738 treatment in the cortex. ELISA quantification of amyloid 1–42 (A) and the ratio of 42/40 are displayed in (B). Levels of both are significantly reduced after ACY-738 treatment and are displayed in picograms per milliliter. n = 5 per group, one-way ANOVA was performed with Turkey's comparisons. *$P < .05$, **$P < .01$, ***$P < .001$. Abbreviations: ELISA, enzyme-linked immunosorbent assay; ANOVA, analysis of variance; WT, wild-type; APP, amyloid precursor protein.

better the prognosis, thus specificity to the class I HDACs has been the focus of cancer therapy with the challenge of trying to limit off-target effects to class II HDACs. Some side effects that have been reported in humans include fatigue, confusion, and mild hepatotoxicity [40]. However, modulation of HDACs in general is always dose dependent

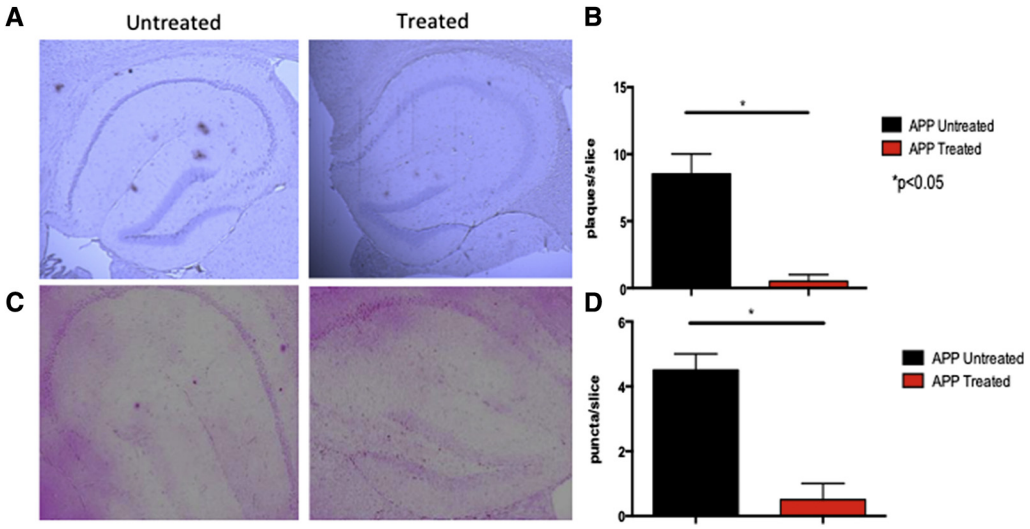

Fig. 6. Representative images from APP-untreated and APP-treated mice from the late treatment group stained with an amyloid beta antibody (A). Quantification of plaques is represented as plaque per slice (B). Representative images from Congo red staining are displayed (C). Quantification of puncta (neuritic plaque cores) is represented as puncta per slice (D). n = 3 per group and *t* tests were performed between APP-treated and APP-untreated groups. *$P < .05$. Abbreviation: APP, amyloid precursor protein.

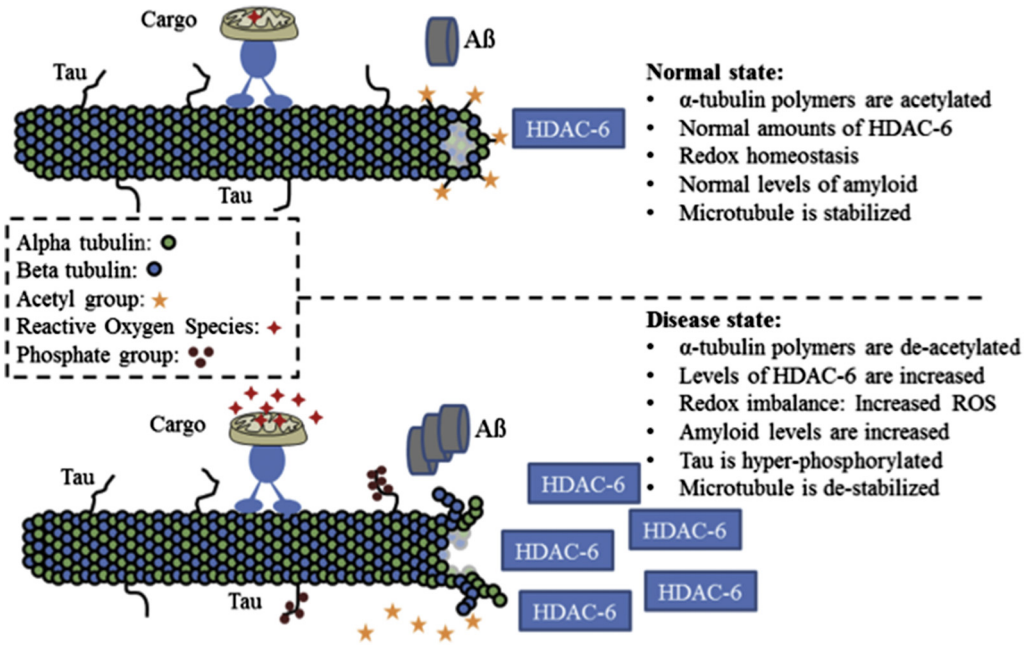

Fig. 7. A hypothetical model is displayed for microtubules in both normal and diseased states. Alterations in the diseased state include increased levels of HDAC6, increases in amyloid, ROS levels, and posttranslational modifications to both tau and tubulin. Abbreviations: HDAC6, histone deacetylase 6; ROS, reactive oxygen species.

and compounds with this selectivity for HDAC-6 inhibition have not been tested in clinical trials.

Modulating HDAC6, a member of the class II family, has shown promise in preclinical trials for neurodegenerative diseases. Specifically, HDAC6 is mainly cytoplasmic, and targets α-tubulin primarily. In mouse models knocking out HDAC-6, mice are normal throughout development. Because of the two catalytic domains present in HDAC6, the off-target effects are limited [41]. The primary roles of HDAC6 are within the microtubule network and in response to accumulation of misfolded proteins. Specifically, HDAC6 plays roles in autophagy and the induction of heat shock proteins to assist with active transport to the aggresome. There is also evidence of deacetylation of two antioxidant enzymes known as peroxiredoxins. This allows the promotion of neurite growth and protection against oxidative stress. Finally, tau can play both an inhibitory and enhancing role in HDAC6 within the microtubules [42]. It is possible that this allows for acute and initial inhibition by HDAC6 and then a modulation of autophagic processes in the brain.

Some potential off-target effects of HDAC6 inhibitors is the induction of apoptosis and T-cell immune response. These can be circumvented with specific dose-dependent regulation and selectivity within the tubulin deacetylation catalytic domain of HDAC6 [43].

Recent evidence and studies involving other commercially available HDAC6 inhibitors have been delivered intravenously with a range of effects on amyloid and tau pathology [23,24,28]. Particularly, tubastatin has been demonstrated to have affects on tubulin acetylation in the brain as well as interact with tau pathology in a recent in vivo study [44]. However, none of the previous studies have delivered HDAC6 inhibitors orally demonstrating both functional axonal transport improvements and changes in PTMs of tau pathology. Diet-based delivery is advantageous in that it easily translates to delivery in the patient. We have shown that ACY-738 can reach therapeutic levels in our organ of interest (brain) and submit that this is particularly advantageous for future work. However, a limitation of this study is duplication of these results in a tau model, which is also applicable to other relevant forms of dementia and AD pathology within the brain.

The role of axonal transport deficits as an early indicator of neuronal damage as well as a link between both amyloid and tau pathology have been established both in vitro and in vivo in a number of models of neurodegenerative diseases [11,18,45]. However, this study is a comprehensive evaluation of a novel pharmacologic compound demonstrating robust improvement using MEMRI as an in vivo methodology in the APP/PS1 mouse model. Beyond preclinical models, axonal transport has been measured ex vivo in a number of brain samples from patients with AD, primarily by measuring the transport rates of vital organelles such as mitochondria [46,47]. Although our methodology for measuring axonal transport rates is not specific to organelle transport, the link between the normalization of mitochondrial dynamics, increase in motor protein function, and improved transport rate has been previously established [8–10,47–49].

Our study also confirmed a number of relationships between PTMs of tau, tubulin, and HDAC6. Previous studies have indicated that HDAC6 interacts with tau and is primarily responsible for the regulation of acetylated tubulin [19,21,50]; however, recent work indicates that some of these interactions may be selectively inhibited. For example, studies that have used tubastatin A and other similar inhibitors have been met with limited success due to the pharmacokinetics of these inhibitors as well as the limited potency in the brain, whereas ACY-738 demonstrates a highly specific and potent presence in brain tissue. Additionally, although the acetylation of tubulin is affected when delivered to tau models [22,51], there are limited effects on the amyloid clearance potential of these inhibitors. Our study indicates that inhibiting HDAC6 using ACY-738 may be effective both at early and late stages of disease progression as well as help reduce some of the amyloid levels in the brain. However, a limitation of the study is the measurement of a single hyperphosphorylated tau epitope, pSer262, which was chosen as the most relevant location for HDAC6 to interact, based on previous literature. Other epitopes (pSer202, pT149, and so forth) did not display significant differences (data not shown), indicating HDAC6 inhibition via ACY-738 may be preferential to pSer262 binding.

In addition to the extension of axonal transport characterization in this study, we also find that ACY-738 treatment effects hyperactivity, and fear-associated learning and memory. This is indicative of an improvement in some of the cognitive processes and phenotypes just before the onset of amyloid pathology in this mouse model. We interpret this modest increase in associative fear conditioning to the nature of variation in consumption of ACY-738 between groups. The WT-treated mice display a 20% freezing rate and the improvement is 25% for the APP-treated group, which could be due to the nature of the variation in chow consumption and acute plasma elevation level within the WT group. We find the WT mice also to have slight elevations in oxidative stress, which do not affect amyloid pathology but could account for limited freezing. In addition, we observe a significant reduction in the soluble amyloid 42/40 ratio, often a clinically relevant outcome used in patient studies. The insoluble ratio remains unchanged in all groups, which may be due to the lack of sensitivity of this particular ELISA with small changes in insoluble Aβ. The APP/PS1 model used in this study has very few plaque deposits at age 6 months, and it is possible the plaques that are visualized in this study are not fully neuritic or insoluble until later in the progression of the disease. However, we do observe a significant reduction in plaque load in the APP-treated groups, indicating that it is possible to recover aggregated forms of Aβ with ACY-738 treatment. However, more studies must be completed to know the effects of long-term treatment with ACY-738 and its effect on aggresome formation to fully elucidate this mechanism of improvements.

Our current work demonstrates that assessing axonal transport rates using MEMRI can be used as both an early indicator of decline and an early output measure of improvement and that this is not only reflected through short-term behavioral improvements but also through PTMs of tau and tubulin. Additionally, we find that amyloid pathology is altered and improved in the hippocampus with an extended treatment at a later stage of amyloid accumulation in the APP/PS1 mouse model. Previous studies have indicated that HDAC6 may play a role in autophagosome formation [21], which warrant additional investigation after treatment with ACY-738, along with specificity of this inhibitor to be effective acutely or over time in other models of AD or related dementias.

Acknowledgments

The authors acknowledge the following individuals for their help and guidance throughout various aspects of this project: Taeko Inoue, Rita Czako, and Loredana Stoica. Additionally, experiments for contextual fear conditioning and immunohistochemistochemical analysis were completed with the assistance of the Costa-Mattioli behavioral suite and the RNA in situ hybridization core under the direction of Drs. Cecilia L. and Roy S.

Supplementary data

Supplementary data related to this article can be found at http://dx.doi.org/10.1016/j.trci.2015.08.001.

RESEARCH IN CONTEXT

1. Systematic Review: Our work investigates a novel, potent, specific HDAC6 inhibitor developed by Acetylon Pharmaceuticals in a preclinical proof of concept study for Alzheimer's disease (AD). Recent studies have investigated conventional HDAC6 inhibitors such as tubacin and tubastatin A with limited success because of lack of blood-brain barrier penetration and toxicity.
2. Interpretation: Our study builds on previous work in AD models using manganese-enhanced magnetic resonance imaging as a noninvasive, longitudinal measurement of in vivo axonal transport using genetic overexpression models. In addition to this, we submit this study as the first to effectively demonstrate the oral delivery of ACY-738 in a mouse model of AD.
3. Future Directions: In the future, more investigation into the mechanisms of uptake and consistency of results in other models of AD are necessary to move this compound into clinical trials.

References

[1] Alzheimer's Association. Alzheimer's Disease Facts and Figures. Alzheimers Dement. 2014;10:e47-92.

[2] Fiandaca MS, Mapstone ME, Cheema AK, Federoff HJ. The critical need for defining preclinical biomarkers in Alzheimer's disease. Alzheimers Dement 2014;10:S196–212.

[3] Carter MD, Simms GA, Weaver DF. The development of new therapeutics for Alzheimer's disease. Clin Pharmacol Ther 2010; 88:475–86.

[4] Savage MJ, Gingrich DE. Advances in the development of kinase inhibitor therapeutics for Alzheimer's disease. Drug Dev Res 2009; 70:125–44.

[5] Stokin GB, Goldstein LS. Axonal transport and Alzheimer's disease. Annu Rev Biochem 2006;75:607–27.

[6] Stokin GB, Lillo C, Falzone TL, Brusch RG, Rockenstein E, Mount SL, et al. Axonopathy and transport deficits early in the pathogenesis of Alzheimer's disease. Science 2005;307:1282–8.

[7] Kanaan NM, Pigino GF, Brady ST, Lazarov O, Binder LI, Morfini GA. Axonal degeneration in Alzheimer's disease: When signaling abnormalities meet the axonal transport system. Exp Neurol 2013; 246:44–53.

[8] Chevalier-Larsen E, Holzbaur EL. Axonal transport and neurodegenerative disease. Biochim Biophys Acta 2006;1762:1094–108.

[9] Brunden KR, Yao Y, Potuzak JS, Ferrer NI, Ballatore C, James MJ, et al. The characterization of microtubule-stabilizing drugs as possible therapeutic agents for Alzheimer's disease and related tauopathies. Pharm Res 2011;63:341–51.

[10] Ballatore C, Brunden KR, Huryn DM, Trojanowski JQ, Lee VM, Smith AB. Microtubule stabilizing agents as potential treatment for Alzheimer's disease and related neurodegenerative tauopathies. J Med Chem 2012;55:8979–96.

[11] Bertrand A, Khan U, Hoang DM, Novikov DS, Krishnamurthy P, Rajamohamed Sait HB, et al. Non-invasive, in vivo monitoring of neuronal transport impairment in a mouse model of tauopathy using MEMRI. Neuroimage 2013;64:693–702.

[12] Smith KD, Kallhoff V, Zheng H, Pautler RG. In vivo axonal transport rates decrease in a mouse model of Alzheimer's disease. Neuroimage 2007;35:1401–8.

[13] Majid T, Ali YO, Venkitaramani DV, Jang MK, Lu HC, Pautler RG. In vivo axonal transport deficits in a mouse model of frontotemporal dementia. Neuroimage Clin 2014;4:711–7.

[14] Inoue T, Majid T, Pautler RG. Manganese enhanced MRI (MEMRI): Neurophysiological applications. Rev Neurosci 2011;22:675–94.

[15] Sharma R, Buras E, Terashima T, Serrano F, Massaad CA, Hu L, et al. Hyperglycemia induces oxidative stress and impairs axonal transport rates in mice. PLoS One 2010;5:e13463.

[16] Massaad CA, Pautler RG. Manganese-enhanced magnetic resonance imaging (MEMRI). Methods Mol Biol 2011;711:145–74.

[17] Massaad CA, Amin SK, Hu L, Mei Y, Klann E, Pautler RG. Mitochondrial superoxide contributes to blood flow and axonal transport deficits in the Tg2576 mouse model of Alzheimer's disease. PLoS One 2010; 5:e10561.

[18] Smith KD, Peethumnongsin E, Lin H, Zheng H, Pautler RG. Increased human wildtype tau attenuates axonal transport deficits caused by loss of APP in mouse models. Magn Reson Insights 2010;4:11–8.

[19] Cook C, Stankowski JN, Carlomagno Y, Stetler C, Petrucelli L. Acetylation: A new key to unlock tau's role in neurodegeneration. Alzheimers Res Ther 2014;6:29.

[20] Odagiri S, Tanji K, Mori F, Miki Y, Kakita A, Takahashi H, et al. Brain expression level and activity of HDAC6 protein in neurodegenerative dementia. Biochem Biophys Res Commun 2013;430:394–9.

[21] Zhang L, Sheng S, Qin C. The role of HDAC6 in Alzheimer's disease. J Alzheimers Dis 2013;33:283–95.

[22] Perez M, Santa-Maria I, Gomez de Barreda E, Zhu X, Cuadros R, Cabrero JR, et al. Tau—an inhibitor of deacetylase HDAC6 function. J Neurochem 2009;109:1756–66.

[23] Govindarajan N, Rao P, Burkhardt S, Sananbenesi F, Schlüter OM, Bradke F, et al. Reducing HDAC6 ameliorates cognitive deficits in a mouse model for Alzheimer's disease. EMBO Mol Med 2013; 5:52–63.

[24] Zhang L, Liu C, Wu J, Tao JJ, Sui XL, Yao ZG, et al. Tubastatin A/ACY-1215 improves cognition in Alzheimer's disease transgenic mice. J Alzheimers Dis 2014;41:1193–205.

[25] Shah SB, Nolan R, Davis E, Stokin GB, Niesman I, Canto I, et al. Examination of potential mechanisms of amyloid-induced defects in neuronal transport. Neurobiol Dis 2009;36:11–25.

[26] Onishi T, Matsumoto Y, Hattori M, Obayashi Y, Nakamura K, Yano T, et al. Early-onset cognitive deficits and axonal transport dysfunction in P301S mutant tau transgenic mice. Neurosci Res 2014;80:76–85.

[27] Selenica ML, Benner L, Housley SB, Manchec B, Lee DC, Nash KR, et al. Histone deacetylase 6 inhibition improves memory and reduces total tau levels in a mouse model of tau deposition. Alzheimers Res Ther 2014;6:12.

[28] Santo L, Hideshima T, Kung AL, Tseng JC, Tamang D, Yang M, et al. Preclinical activity, pharmacodynamic, and pharmacokinetic properties of a selective HDAC6 inhibitor, ACY-1215, in combination with bortezomib in multiple myeloma. Blood 2012;119:2579–89.

[29] D' Ydewalle C, Krishnan J, Chiheb DM, Van Damme P, Irobi J, Kozikowski AP, et al. HDAC6 inhibitors reverse axonal loss in a mouse model of mutant HSPB1-induced Charcot-Marie-Tooth disease. Nat Med 2011;17:968–74.

[30] Peethumnongsin E, Yang L, Kallhoff-Munoz V, Hu L, Takashima A, Pautler RG, et al. Convergence of presenilin- and tau-mediated pathways on axonal trafficking and neuronal function. J Neurosci 2010; 30:13409–18.

[31] Manuchehrfar F, Shamloo A, Mehboudi N. Dynamic response of axonal microtubules under suddenly applied end forces. Conf Proc IEEE Eng Med Biol Soc 2014;2014:6183–6.

[32] Medway C, Morgan K. Review: The genetics of Alzheimer's disease; putting flesh on the bones. Neuropathol Appl Neurobiol 2014; 40:97–105.

[33] Herrup K, Carrillo MC, Schenk D, Cacace A, Desanti S, Fremeau R, et al. Beyond amyloid: Getting real about nonamyloid targets in Alzheimer's disease. Alzheimers Dement 2013;9:452–4581.

[34] Dai J, Buijs RM, Kamphorst W, Swaab DF. Impaired axonal transport of cortical neurons in Alzheimer's disease is associated with neuropathological changes. Brain Res 2002;948:138–44.

[35] Jankowsky JL, Fadale DJ, Anderson J, Xu GM, Gonzales V, Jenkins NA, et al. Mutant presenilins specifically elevate the levels of the 42 residue beta-amyloid peptide in vivo: Evidence for augmentation of a 42-specific gamma secretase. Hum Mol Genet 2004;13:159–70.

[36] Huang W, Zhu PJ, Zhang S, Zhou H, Stoica L, Galiano M, et al. mTORC2 controls actin polymerization required for consolidation of long-term memory. Nat Neurosci 2013;16:441–8.

[37] Sbarbati A, Calderan L, Nicolato E, Marzola P, Lunati E, Donatella B, et al. Magnetic resonance imaging of the rat Harderian gland. J Anat 2002;201:231–8.

[38] Akins MR, Greer CA. Cytoskeletal organization of the developing mouse olfactory nerve layer. J Comp Neurol 2006;494:358–67.

[39] Kim J, Choi IY, Michaelis ML, Lee P. Quantitative in vivo measurement of early axonal transport deficits in a triple transgenic mouse model of Alzheimer's disease using manganese-enhanced MRI. Neuroimage 2011;56:1286–92.

[40] Wagner JM, Hackanson B, Lübbert M, Jung M. Histone deacetylase (HDAC) inhibitors in recent clinical trials for cancer therapy. Clin Epigenetics 2010;1:117–36.

[41] Gräff J, Tsai LH. The potential of HDAC inhibitors as cognitive enhancers. Annu Rev Pharmacol Toxicol 2013;53:311–30.

[42] Dallavalle S, Pisano C, Zunino F. Development and therapeutic impact of HDAC6-selective inhibitors. Biochem Pharmacol 2012; 84:756–65.
[43] Simões-Pires C, Zwick V, Nurisso A, Schenker E, Carrupt PA, Cuendet M. HDAC6 as a target for neurodegenerative diseases: What makes it different from the other HDACs? Mol Neurodegener 2013;8:7.
[44] Sung YM, Lee T, Yoon H, DiBattista AM, Song JM, Sohn Y, et al. Mercaptoacetamide-based class II HDAC inhibitor lowers Aβ levels and improves learning and memory in a mouse model of Alzheimer's disease. Exp Neurol 2013;239:192–201.
[45] Shaw JL, Chang KT. Nebula/DSCR1 upregulation delays neurodegeneration and protects against APP-induced axonal transport defects by restoring calcineurin and GSK-3β signaling. PLoS Genet 2013; 9:e1003792.
[46] Baloyannis SJ. Mitochondrial alterations in Alzheimer's disease. J Alzheimers Dis 2006;9:119–26.
[47] Hollenbeck PJ, Saxton WM. The axonal transport of mitochondria. J Cell Sci 2005;118:5411–9.
[48] Stokin GB, Goldstein LS. Linking molecular motors to Alzheimer's disease. J Physiol Paris 2006;99:193–200.
[49] Kuznetsov AV. Comparison of active transport in neuronal axons and dendrites. Math Biosci 2010;228:195–202.
[50] Cook C, Carlomagno Y, Gendron TF, Dunmore J, Scheffel K, Stetler C, et al. Acetylation of the KXGS motifs in tau is a critical determinant in modulation of tau aggregation and clearance. Hum Mol Genet 2014; 23:104–16.
[51] Noack M, Leyk J, Richter-Landsberg C. HDAC6 inhibition results in tau acetylation and modulates tau phosphorylation and degradation in oligodendrocytes. Glia 2014;62:535–47.